Synthesis, Characterization and Optoelectronic Property of Axial-Substituted Subphthalocyanines

Zhuo Li,*[a, b, d] Bing Wang,[a] Bingbing Zhang,[a] Guoyi Cui,[a] Fenyan Zhang,[c] Long Xu,[a] Linyu Jiao,[a] Lingyan Pang,[e] and Xiaoxun Ma*[a, d]

Two novel substituted subphthalocyanines have been prepared introducing m-hydroxybenzoic acid and m-hydroxyphenylacetic acid into the axial position of bromo-subphthalocyanine. The compounds have been characterized by Fourier transform infrared (FT-IR), Nuclear Magnetic Resonance (NMR) and single-crystal X-rays diffraction (XRD) methods. Their photophysical properties show that the axial substitution results into a relatively higher fluorescence quantum efficiency ($\Phi_F = 5.74$ for m-hydroxybenzoic acid and 9.09% for m-hydroxyphenylacetic acid) in comparison with that of the prototype compound, despite the almost negligible influence on the maximum absorption or the emission position. Moreover, the electrochemical behaviors show that the axial-substituted subphthalocyanines also exhibit enhanced specific capacitances of 395 F/g (m-hydroxybenzoic acid) and 362 F/g (m-hydroxyphenylacetic acid) compared with 342 F/g (the prototype) to the largest capacitance at the scan rate of 5 mV/s, and the significantly larger capacitance retentions of 83.6% and 82.1% versus 37.3% upon density up to 3 A/g. These results show the potential of these axial-substituted subphthalocyanines in the use as organic photovoltaics and supercapacitors.

1. Introduction

The development of high-performance organic materials with extensive applications has become an important field of research.[1] Recently, the interest on subphthalocyanine (SubPc) and their derivatives has been enlarged because of their multiple technological applications which include organic optoelectronics[2,3,4]. As a typical phthalocyanine compound, the SubPc consists of three isoindole units and has a delocalized 14 π-electrons conjugation system, processing a conical bowl-shaped structure with non-central symmetry[5]. This unique structural features confer good chemical stability and high thermal stability, thus making these molecules attractive tools for optoelectronic applications[6] such as nonlinear optics[7], organic light emitting diodes[8] and organic photovoltaics[9] with electron-transfer processes[10]. In particular, those studies aimed

at introducing different peripheral or axial substitution in the SubPc to meet the multitudinous optoelectronic needs, have also been receiving considerable attention in the past few years[11]. As a matter of fact, incorporating molecular fragments in an axial position has some additional technological advantages. Besides the avoiding the tedious synthetic routes leading to unsymmetrically equator-substituted SubPcs[12], the persisting macrocycle within the axial substitution SubPcs can hold the intrinsic electronic character and the desirably high stability of the SubPc. From the viewpoint of axial modification, the traditional method is to replace the original axial Cl (and sometimes Br) atom towards the corresponding derivatives, where different functional ligands including pseudohalides[12,13], nucleophiles[14,15] and oxygen-bearing nucleophiles[16] are commonly adopted, affording various axial derivatives for photoelectric devices[17]. Undoubtedly, either the peripheral or the axial substituting should provide the SubPc-derivatives with similar photo-physical and electrochemical properties to that of the original SubPc. Nonetheless, to the best of our knowledge, the structural effect of different SubPc-derivatives involving both peripheral and axial ligands on the fine-tuning photophysical or electrochemical properties is rarely reported. Possibly this is due to the difficulties encountered in their separation and purification[18,19]. In this work, the preparation of two novel axial-substituted SubPcs by solvent-thermal method is reported. The compounds have been synthesized introducing m-hydroxybenzoic acid or m-hydroxyphenylacetic acid into the axial position of bromo-SubPc. After isolation, the purified two axial-substituted SubPcs were well-characterized by FT-IR, NMR and single-crystal X-rays diffraction (XRD) analyses. Moreover, the comparison of their photophysical and electrochemical properties with those of the bromo-SubPc is reported.

[a] Dr. Z. Li, B. Wang, B. Zhang, G. Cui, Prof. L. Xu, Dr. L. Jiao, Prof. X. Ma
School of Chemical Engineering, Northwest University, Shaanxi, Xi'an, 710069 (China)

[b] Dr. Z. Li
Department of Chemistry and Centre for Plastic Electronics, Imperial College London, Exhibition Road, London SW7 2AZ, UK

[c] F. Zhang
College of food science and technology, Northwest University, Shaanxi, Xi'an, 710069 (China)

[d] Dr. Z. Li, Prof. X. Ma
Chemical Engineering Research Center of the Ministry of Education for Advanced Use Technology of Shanbei Energy, Shaanxi Research Center of Engineering Technology for Clean Coal Conversion, Northwest University, Xi'an, 710069 (China)

[e] Dr. L. Pang
School of Materials Science and Engineering, Shaanxi University of Science and Technology, Xi'an 710021 (China)

ChemistryOpen

Full Papers
doi.org/10.1002/open.202000206

Chemistry Europe
European Chemical
Societies Publishing

Experimental Section

Materials

All the chemical reagents used in the experiment were analytically pure. Boron tribromide (BBr$_3$), o-dicyanobenzene, m-hydroxybenzoic acid and m-hydroxyphenylacetic acid were all procured from Bailingwei Technology Co Ltd. Toluene and anhydrous ethanol were procured from Tianjin Fuyu Chemical Co Ltd. Nickel foam, potassium hydroxide (KOH) and black carbon are purchased from Xi'an Kohao.

Characterization Methods

Elemental (C, H, N) analyses of the compounds were performed with a Vario EL III CHNOS analyzer. FT-IR spectra (resolution 4 cm^{-1}, substrate KBr) was recorded on a Bruker Vector 22 FT-IR spectrometer (4000–400 cm^{-1}). ^{1}H NMR spectra recorded on a JEOL ECZ600R spectrometer and ^{13}C NMR spectral measurements with a JEOL EX-150 spectrometer were performed in DMSO-d_6 at room temperature. UV-Vis absorption spectrum and fluorescence spectra were performed to represent the optical properties of the compounds obtained in chloroform solvent using a Horiba Fluorolog-3 spectrometer at a range of 200–800 nm.

Syntheses

Synthesis of the Bromo-Subphthalocyanine H$_{12}$SubPcB-Br (SH0)

The synthetic pathway to the compounds was shown in Figure 1. Dry 1, 2-dicyanobenzene (10 mmol) was first added into a relevant 100-mL three-necked flask under the protection of N$_2$, and then 40 mL 1, 2-dichlorobenzene was injected into the system. The resulting mixture was continuously stirred at room temperature to distribute the ingredients evenly. BBr$_3$ (2.0 mL) was further added, and the mixture was heated and kept stirring under reflux for 12 h. During the reaction, the color of the reaction system was changed from reddish brown to purple. After cooling to room temperature, the solvent was removed by vacuum distillation and the residual crude was recrystallized with ethanol, giving the micro-crystalline product. For the SH0 (H$_{12}$SubPcB–Br): Yield: 0.396 g (25% based on phthalonitrile). M.p. > 300 °C. Elemental Anal. Calcd (%) for C$_{24}$H$_{12}$BBrN$_6$: C, 60.67; H, 2.55; N, 17.69. Found: C, 60.65; H, 2.55; N, 17.71. FT-IR data (KBr, cm^{-1}): 3427.21, 1600.88, 1565.04, 1450.29, 1379.88, 1282.28, 1232.44, 1199.22, 1131.38, 948.30, 875.27, 746.53, 692.19, 621.32, 562.41, 510.49 and 440.58. ^{1}H NMR (600 MHz, DMSO-d_6): δ (ppm) 8.92 (dd, 6H, –Ph), 7.85 (dd, 6H, –Ph). ^{13}C NMR (150 MHz, DMSO-d_6): δ (ppm) 166.7, 156.8, 131.4, 129.0, 119.4, 115.2.

Synthesis of the Axial Substituted Subphthalocyanine H$_{12}$SubPcB-OPhCOOH (SH1)

To a tank containing 0.15 mmol (16.2 mg) m-hydroxybenzoic acid, 6 mL toluene and a drop of pyridine, 47.5 mg H$_{12}$SubPcB–Br was added. The resulting mixture was treated under an ultrasonic condition for 2 h and then put into the oven. When the oven temperature was up to 110 °C in 2 h, it was kept at 110 °C for another 20 h. After cooling to room temperature within 55 h, the reaction tank was taken out and filtered. The filtrate was transferred into a small beaker and slowly evaporated at room temperature, affording to a bright purple micro-crystalline product. For the SH1 (H$_{12}$SubPcB–OPhCOOH): Yield: 29.4 mg (55% based on the SH0). M.p. > 300 °C. Elemental Anal. Calcd (%) for C$_{31}$H$_{17}$BN$_6$O$_3$: C, 69.95; H, 3.22; N, 15.79. Found: C, 69.91; H, 3.23; N, 15.76. FT-IR data (KBr, cm^{-1}): 2990.37, 1706.76, 1602.54, 1587.56, 1455.38, 1436.42, 1388.64, 1286.10, 1235.17, 1198.03, 1170.76, 1155.96, 1133.29, 1049.49, 1000.15, 920.95, 883.81, 811.88, 783.83, 759.94, 731.12, 695.54, 673.47 and 653.47. ^{1}H NMR (600 MHz, DMSO-d_6): δ (ppm) 12.43 (–COOH), 8.80 (dd, 6H, –Ph), 7.96 (dd, 6H, –Ph), 7.02 (t, 2H, –Ph), 6.77 (t, 2H, –Ph). ^{13}C NMR (150 MHz, DMSO-d_6): δ (ppm) 169.1 (COOH), 167.1, 161.5, 150.5, 134.2, 132.5, 131.4, 129.7, 128.8, 128.1, 122.8, 121.7, 115.0 (CO).

Synthesis of the Axial Substituted Subphthalocyanine H$_{12}$SubPcB-OPhCH$_2$COOH (SH2)

The synthesis of the SH2 was in the same way as the SH1 except that m-hydroxyphenylacetic acid (0.15 mmol, 20.41 mg) instead of m-hydroxybenzoic acid (0.15 mmol, 16.2 mg) was used. For the SH2 (H$_{12}$SubPcB–OPhCH$_2$COOH): Yield: 37.7 mg (69% based on the SH0). M.p. > 300 °C. Elemental Anal. Calcd (%) for C$_{32}$H$_{19}$BN$_6$O$_3$: C, 70.35; H, 3.51; N, 15.38. Found: C, 70.31; H, 3.50; N, 15.41. FT-IR data (KBr, cm^{-1}): 3192.60, 2980.52, 1724.20, 1600.49, 1456.82, 1378.60, 1284.13, 1229.39, 1134.92, 1055.94, 875.68, 746.16, 709.80, 687.84 and 647.70. ^{1}H NMR (600 MHz, DMSO-d_6): δ (ppm) 12.74 (s, 1H, -COOH), 8.83 (m, 6H, –Ph), 7.97 (m, 6H, –Ph), 7.04 (t, 2H, –Ph), 6.69 (t, 2H, –Ph), 5.19 (m, 2H, -CH$_2$). ^{13}C NMR (150 MHz, DMSO-d_6): δ (ppm) 173.3 (COOH), 169.4, 156.2, 151.3, 134.5, 132.8, 130.4, 130.3, 129.1, 128.4, 125.3, 123.1, 115.1 (CO), 49.2 (CH$_2$).

Crystal Structure Determination

Crystallographic data of SH0, SH1·H$_2$O and SH2·H$_2$O were collected at 296(2) K on a Bruker Apex II CCD diffractometer with 50 kV using Mo Kα ($\lambda = 0.71073$ Å) radiation. The structures were determined by direct methods and refined by full-matrix least-square on F^2 using the SHELXL-97 program package. All the non-hydrogen atoms were refined with anisotropic displacement parameters. Hydrogen atoms connected to carbon were located in geometrically idealized positions and refined by a riding model. CCDC numbers of 1960643
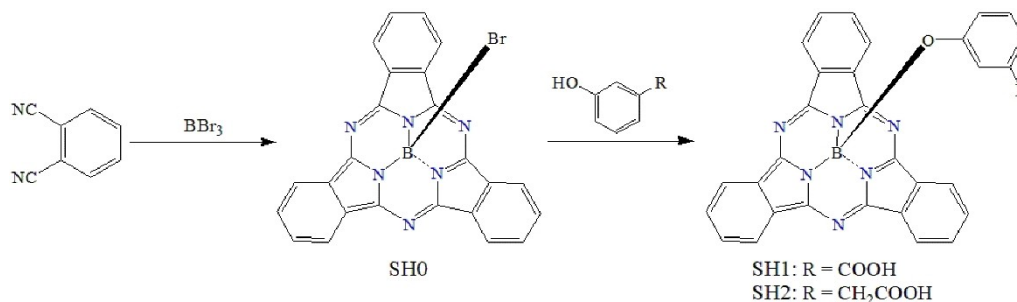

Figure 1. The synthetic route of SH0, SH1 and SH2.

ChemistryOpen

Full Papers
doi.org/10.1002/open.202000206

Chemistry Europe
European Chemical
Societies Publishing

for the SH0 and 1978658–1978659 for complexes SH1·H$_2$O and SH2·H$_2$O.

Electrochemical Methods

Electrochemical property measurements were carried out with a traditional three-electrode system, where a platinum plate as a counter electrode, a saturated calomel electrode (SCE) as a reference electrode and the prepared material as the working electrode with 1.5 mg active substance were adopted, respectively. All tests were employed a 6 mol/L KOH solution as the electrolyte. Cyclic Voltammetry (CV) and Galvanostatic Charging/Discharging techniques (GCD) testing were executed at different scan rates and different current densities, respectively. Electrochemical Impedance Spectroscopy (EIS) test was carried out in the frequency range of 0.01 Hz ~ 100 kHz with an amplitude of 5 mV. The specific capacitance (Cm (F/g)) is calculated using the following expression (1):

$$C_{sp} = \frac{C}{m} = \frac{I \times \Delta t}{\Delta V \times m} \tag{1}$$

Where I (A) is the discharge current; m (g) is the mass of the active material coated on the foamed nickel; Δt (s) is the discharge time; and ΔV (V) is the potential change of discharge process.

Table 1. Crystallographic data of compounds SH0, SH1·H$_2$O and SH2·H$_2$O

complex	SH0	SH1·H$_2$O	SH2·H$_2$O
formula	C$_{24}$H$_{12}$BBrN$_6$	C$_{31}$H$_{19}$BN$_6$O$_4$	C$_{32}$H$_{21}$BN$_6$O$_4$
formula weight	475.12	568.0	564.36
T/K	293(2)	296(2)	296(2)
crystal system	Orthorhombic	Triclinic	Monoclinic
space group	Pnma	P-1	P2(1)/n
a/Å	12.183(9)	9.0467(18)	10.568(7)
b/Å	15.101(7)	12.868(3)	14.735(10)
c/Å	10.502(5)	12.992(3)	17.320(12)
α/°	90.00	106.87(3)	90
β/°	90.00	108.92(3)	94.087(13)
γ/°	90.00	99.41(3)	90
V/ Å^3	1932.28(19)	1312.7(9)	2690(3)
Z	4	2	4
D/g·cm^{-3}	1.633	1.438	1.393
F(000)	952	588	1168
data/restraints/Parameters	1721/0/151	5475/1/392	4797/0/390
Goodness-of-fit on F^2	0.993	0.927	1.028
R$_1$^{a} [I > 2σ(I)]	0.0692	0.0865	0.0777
wR$_2$^{a} [I > 2σ(I)]	0.1835	0.2121	0.2075
R$_1$^{a} (all data)	0.0993	0.2352	0.1494
wR$_2$^{a} (all data)	0.2110	0.3043	0.2555
Largest diff peak/hole (e·Å^{-3})	1.032, −0.751	0.331, −0.3043	0.799, −0.479
CCDC No.	1960643	1978658	1978659

^{a}R$_1$ = Σ||Fo| − |Fc||/Σ|Fo|; wR$_2$ = [Σw(F$_o$^{2}–F$_c$^{2})^2/Σw(F$_o$^{2})^2]$^{1/2}$

2. Results and Discussion

2.1. Synthesis and Characterization

Based on the bromo-SubPc (SH0) as the starting material, its treatment with m-hydroxybenzoic acid or m-hydroxyphenylacetic acid by solvent-thermal method, as shown in Figure 1, gives rise to two novel axial-substituted SubPcs SH1 and SH2, respectively. The three compounds SH0, SH1 and SH2 were well-characterized by XRD, FT-IR and ^{1}H/^{13}C NMR methods. Especially in their ^{1}H NMR spectra, the only presence of one set of the SubPc-based proton resonances (δ = 8.92 and 7.85 ppm), indicates their approximate C$_3$ symmetric character upon the axial coordination. Moreover, through the axial substituent of

m-OPhCOOH for SH1 or m-OPhCH$_2$COOH for SH2 in replacement, there has a significant spread shift (δ from 12.43 to 6.77 ppm for SH1 or δ from 12.74 to 5.19 ppm for SH2) relative to that of SH0 with the Br atom at the axial position. The molecular structures of the compounds SH0, SH1·H$_2$O and SH2·H$_2$O were also confirmed by Single-crystal X-ray diffraction (XRD) studies, and the crystallographic data were summarized in Tables 1–2. Figure 2 shows both the top and side views of the host framework of SH0, SH1·H$_2$O or SH2·H$_2$O, where the axial substituent of an −OPhCOOH group for the SH1 and an −OPhCH$_2$COOH group for the SH2 in replacement for the Br-group in the SH0 was visibly observed. The center of the SH1 or the SH2 is occupied by one boron atom in a nearly triangular

Table 2. Selected bond length (Å) and bond angle (°) data for SH0, SH1·H$_2$O and SH2·H$_2$O.

| SH0		SH1·H$_2$O		SH2·H$_2$O	
B(1)–N(2)	1.453(7)	O(1)–B(1)	1.446(8)	B(1)–O(1)	1.443(5)
B(1)–N(2)#1	1.453(7)	N(5)–B(1)	1.530(8)	B(1)–N(5)	1.486(5)
B(1)–N(4)	1.477(10)	N(3)–B(1)	1.477(9)	B(1)–N(1)	1.491(6)
B(1)–Br(1)	2.056(9)	N(1)–B(1)	1.487(8)	B(1)–N(2)	1.498(6)
N(2)–B(1)–N(2)#1	106.7(7)	N(4)–C(16)	1.319(7)	N(1)–C(1)	1.367(5)
N(2)–B(1)–N(4)	106.4(5)	N(2)–C(9)	1.343(7)	N(3)–C(24)	1.341(5)
N(2)#1–B(1)–N(4)	106.4(5)	N(3)–B(1)–N(1)	104.8(5)	N(5)–B(1)–N(1)	104.4(3)
N(2)–B(1)–Br(1)	112.8(4)	N(3)–B(1)–N(5)	103.8(5)	N(5)–B(1)–N(2)	103.5(3)
N(2)#1–B(1)–Br(1)	112.8(4)	N(1)–B(1)–N(5)	102.8(5)	N(1)–B(1)–N(2)	103.6(3)
N(1)–C(1)	1.335(6)	O(1)–B(1)–N(3)	117.6(6)	O(1)–B(1)–N(5)	111.8(4)
C(1)–C(2)	1.448(7)	O(1)–B(1)–N(1)	118.7(6)	O(1)–B(1)–N(1)	116.5(4)
C(7)–C(8)	1.461(8)	O(1)–B(1)–N(5)	107.3(5)	O(1)–B(1)–N(2)	115.6(4)
C(9)–C(10)	1.473(8)	O(1)–C(25)	1.375(7)	O(1)–C(26)	1.394(5)
C(1)–N(1)–C(1)#1	117.3(7)	O(3)–C(31)	1.295(8)	O(2)–C(32)	1.162(7)
C(8)–N(2)–C(1)	113.5(5)	O(2)–C(31)	1.258(9)	O(3)–C(32)	1.204(7)
C(8)–N(2)–B(1)	123.0(5)	N(2)–C(8)	1.338(7)	N(1)–C(8)	1.364(5)
C(1)–N(2)–B(1)	122.5(5)	N(4)–C(17)	1.353(7)	N(2)–C(16)	1.357(5)
N(4)–B(1)–Br(1)	111.2(6)	N(6)–C(1)	1.360(7)	N(4)–C(17)	1.338(5)
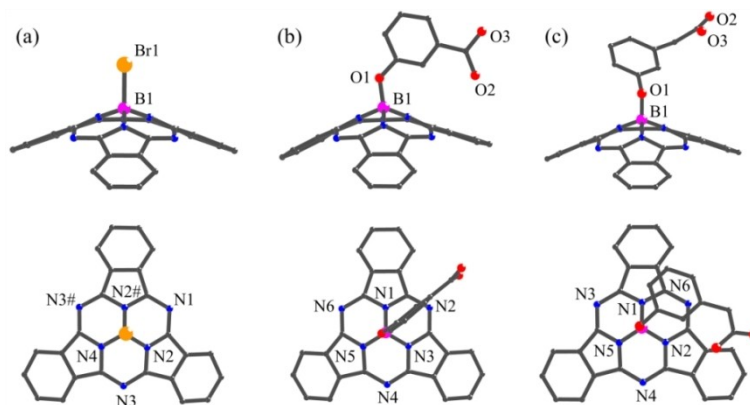
Figure 2. X-ray crystal structure of (a) SH0, (b) SH1 and (c) SH2 (top, side view; bottom, convex view; C, black; N, blue; Br, orange; B, purple; O, red). All the H atoms and solvate H_2O are omitted for clarity.

pyramidal geometry, which is similar to that of the SH0. However, Their detailed difference lies in the different four-coordinate environment of the central B atom in the $3\,N+Br$ mode for SH0 while the $3N+O$ mode for SH1 or the SH2.

Moreover, for the SH0 with one Br atom at the axial position, the B atom is located at the center of the bottom plane with the almost equivalent N—B—N bond angles and the B—Br bond length of 2.056(9) Å. In contrast, for the SH1, although the three coordination N atoms (N1, N3 and N5) are also almost *co*-planar, the central B atom with an axial linkage to one O atom (B—O; 1.446(8) Å) is deviated from the basic plane with a distance of 0.6268(99) Å. Meanwhile, a similar structure character is observed for the SH2, from which, the B—O bond length of 1.443(5) Å and the B-bulged height of 0.6226(50) Å for the *m*-OPhCH$_2$COOH-modified SH2 are in good agreement with those for the SH1 with one *m*-OPhCOOH at the axial position, correspondingly. Worthy of notice, contributing to the axial substituent of the *m*-OPhCH$_2$COOH for the SH2 or the *m*-OPhCOOH the SH1, their relatively longer B—N bond lengths (1.477(9)–1.530(8) Å for the SH1 or 1.486(5)–1.498(6) Å for the SH2) within the equatorial macrocycle plane than those (1.453(7)–1.477(10) Å) of the SH0 are also observed.

In the FT-IR spectra of the three SubPcs, besides the similar C=C- and C=N-characteristic absorptions (Table 3 and Figure 3) of the typical SubPc, the strong C—Br absorption peaking at 621 cm^{-1} is shown for the SH0, while the B—O stretching absorption locates at 1134 cm^{-1} for the SH1 or the SH2. In addition, The absorptions at 1706 cm^{-1} and 1286 cm^{-1} for the SH1 or 1724 cm^{-1} and 1284 cm^{-1} for the SH2 should be assigned to the -COOH-characteristic v_s and v_{as} vibration absorptions, respectively.
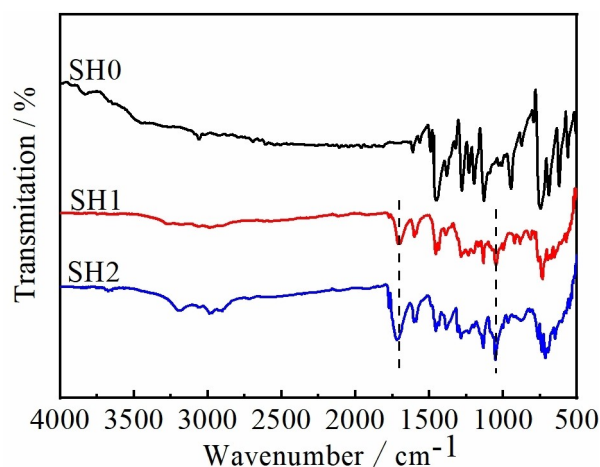

Figure 3. FT-IR spectra of the compounds SH0, SH1 and SH2.

2.2. UV-Visible Absorption and Fluorescent Properties

Figure 4(a) displays the UV-visible absorption spectral result of the three compounds in dilute solution. Clearly, their comparable broad absorption bands are exhibited. The relatively weak band peaking at 305–309 nm and the other strong peak at 563–567 nm should be assigned to the B-band and the Q-band of the typical SubPc[13,21], respectively. In comparison, besides the slight red-shift of the B-band peak, while the minor blue-shift of the Q-band one for the two axial substituted SubPcs SH1 and SH2 compared to the SH0, the significantly lower intensities of both the B and Q bands for the SH1 and SH2 than those of the SH0 are also observed, which is probably resulted from the decreased π-electron conjugation of the SubPc keleton with the axial substituent.

The photo-physical property of the three compounds was further investigated in solution at room temperature, and the result was summarized in Figure 4(b). Even upon photo-excitation at 500 nm, their similar fluorescent behavior can be turned-on, peaking at 586 nm for the SH0, 579 nm for the SH1 or 581 nm for the SH2, respectively. For comparison, the fluorescence quantum yield (Φ_F) was further determined. The
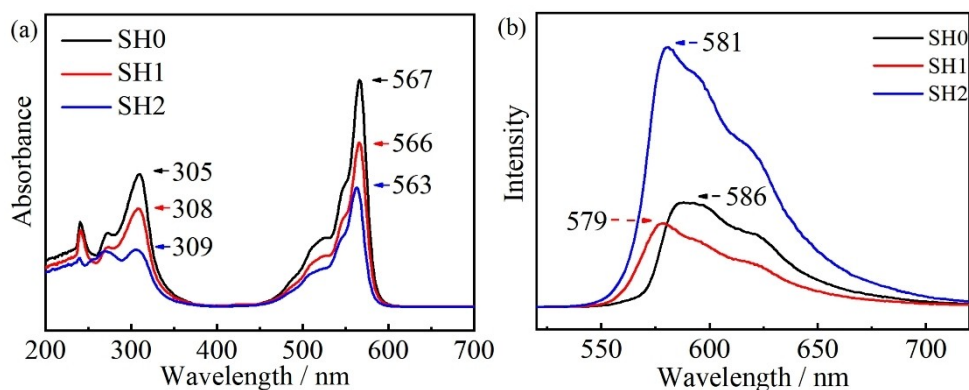
Table 3. The typical absorptions of the compounds SH0, SH1 and SH2

Bonds Materials	C=C (cm^{-1})	C=N (cm^{-1})	B—X (cm^{-1})	Axial substituents (cm^{-1})	
SH0	1600	1450	621	–	–
SH1	1602	1455	1133	1706	1286
SH2	1600	1456	1134	1724	1284

ChemistryOpen

Full Papers
doi.org/10.1002/open.202000206

Chemistry Europe
European Chemical
Societies Publishing

Figure 4. UV-Vis spectra (a) and fluorescence spectra (b; $\lambda_{ex}=500$ nm) of the SH0, the SH1 and the SH2 in chloroform solution.

experimental Φ_F values for the SH0, the SH1 and the SH2 are 2.34%, 5.74% and 9.07%, respectively, from which, the enhanced fluorescent property of the SH1 and the SH2 renders the axial substituted SubPc a potential candidate as an optoelectronic material.

2.3. Electrochemical Properties

In consideration of the unique electrochemical property of SubPc or its derivative, the CV (Figure 5) and GCD (Figure 6) curves of the three compounds were obtained to check their electrochemical characteristics. As shown in Figure 5, because their distinctively separated oxidative and reductive peaks belong to the typical battery behavior, an accurate kinetic calculation is performed using the equation $i=av^b$, proposed by Trasatti and co-workers[20]. It is the value of b to decide the
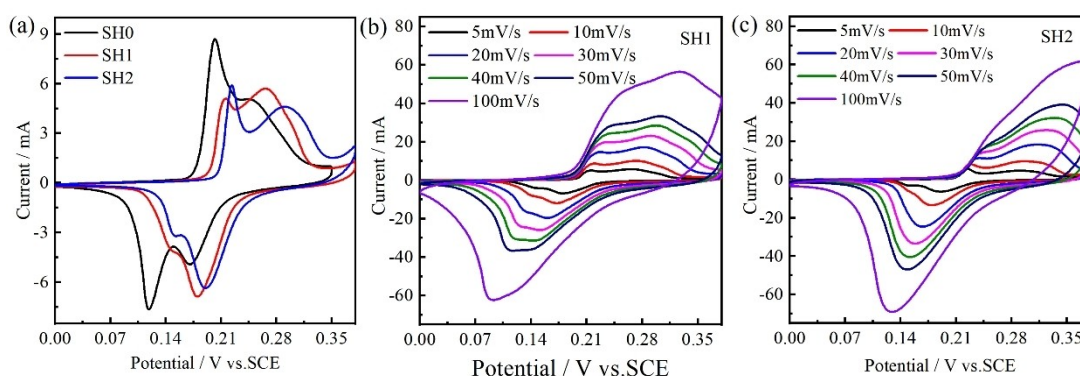

Figure 5. a) CV of the complexes SH0, SH1 and SH2 at a scanning rate of 5 mV/s, (b) CV of SH1 at different rates, (c) CV of SH2 at different rates.
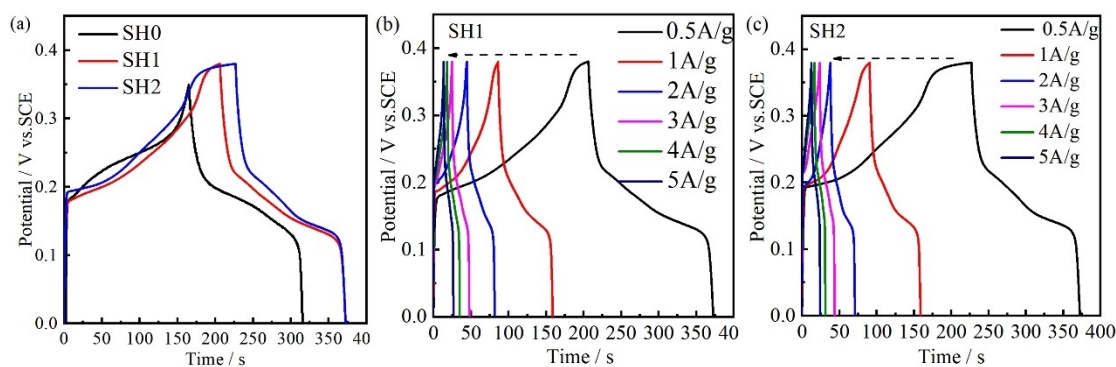

Figure 6. (a) GCD of the complexes SH0, SH1 and SH2 at a current density of 0.5 A/g, (b) GCD of SH1 at different current densities, (c) GCD of SH2 at different current densities.

ChemistryOpen

Full Papers
doi.org/10.1002/open.202000206

Chemistry Europe
European Chemical
Societies Publishing

characteristic feature. The calculated b values lie in the range of 0.5 to 1 (0.80469 for the SH0, 0.71294 for the SH1 and 0.86163 for the SH2). Hence, due to the combination of the diffusion-controlled contribution and capacitive contribution, the three compounds should simultaneously have the battery behavior and pseudo capacitance behavior. In detailed, Figure 5(a) gives a comparison of the cyclic voltammetry (CV) curves of the three compounds at a scanning rate of 5 mV/s with the potential range of 0–0.4 V. The oxidation potentials of the SH1 and the SH2 were 0.215 V and 0.225 V, respectively. Meanwhile, their corresponding reduction potentials of 0.182 V and 0.196 V are calculated, respectively. Compared to SH0, both the oxidation and reduction potentials of the SH1 and the SH2 with the axial substituents apparently move towards more positive values, which is similar to that[21,22] SubPcs with the equatorial substituents. Interestingly, the redox potentials of the SH1 and SH2 are significantly smaller than that ($E^1_{pa,ox}=0.374$ V) of the amino derivative or that ($E^1_{pa,ox}=0.600$ V) of the oxo derivatives[21]. The potential shifts should be relevant to the stronger electron-withdrawing ability with the axial substitutions. Additionally, the integration areas within the current-potential of SH1 and SH2 are slightly larger than that of SH0, revealing that SH1 and SH2 have relatively higher specific capacities and electrochemical reaction activities. The CV voltammograms of the axial-substituted SH1 and SH2 at varied scan rates were further carried out as shown in Figure 5(b) and (c). The obvious redox peaks also exist accompanying the increase of the scan rate, indicating that the two axial substituted compounds have excellent reversibility and multiple rates.

To further evaluate their potential application in terms of the electrochemical behaviors, Galvanostatic Charging/Discharging (GCD) measurements were carried out for at the current density of 0.5 A/g, as shown in Figure 6(a). A charging-discharging process with the pseudo capacitive performance can evidently be verified. Compared with the SH0, the charge and discharge areal capacitance of the SH1 and the SH2 are calculated to be much higher, also confirming that their superior specific capacitances are consistent with the CV results. In the meantime, the GCD curves at various currents ranging from 0.5 A/g to 5 A/g were also displayed in Figure 6(b) and (c).

The two axial-substituted SubPcs still keep the GCD characteristic at 5 A/g, endowing a potential in future energy storage application. According to Formula (1), when current loading increases, the value of I/m increases and the specific capacitance of material (Csp) decreases. The decreased specific capacitanceis mainly attributed to the increased diffusionrate capability and form a concentration polarization with the current loading increase. Hence, the discharging time Δt decrease with increased the current loading when △V remains unchanged.

Through extracting the capacities of the three electrode complexes at different scan rates and current densities, Figure 7(a) and (b) depicted the results. At the same scanning rate, the two axial-substituted compounds have the significantly larger capacitances than that of the SH0. Especially, the largest capacitances for the SH1 and the SH2 are observed to be 395 F/g and 362 F/g at a scan rate of 5 mV/s, respectively. On the other hand, their capacity performance at a progressively increased current density is compared and shown in Figure 7(b), where the capacitance of the SH0 decreases sharply with the increase of current density, while the capacitance of every axial-substituting one can keep its positive value in a higher level and decays much slowly. At 0.5 A/g, the capacitances of the SH0, the SH1 and the SH2 are calculated to be 177 F/g, 219 F/g and 191 F/g, respectively. However, differently from the capacitance retention down to 37.3% for the SH0 at 3 A/g, there has no significant degradation observed for the two axial-substituted compounds, whose 83.6% and 82.1% capacitance retentions can keep the pseudo-capacitive characteristic. Due to the highest specific capacity inversely proportional to the equivalent serial resistance (ESR) including the transport resistances of electrons and ions, the faradaic reaction happens rapidly, and thus the rate capability of the electrode is mainly determined by the transports of electrons and ions[22]. Compared to the SH0, the two axial-substituted SubPc compounds SH1 and SH2 can prevent the blocking of ion channels during the stacking process and facilitate the transport of ions. As a result, both the SH1 and the SH2 are resistant to capacity loss even at higher current loading compared to the SH0.

Figure 8 demonstrated the Nyquist plots' in frequencies ranging from 100 kHz to 0.01 Hz with ac perturbation of 5 mV.
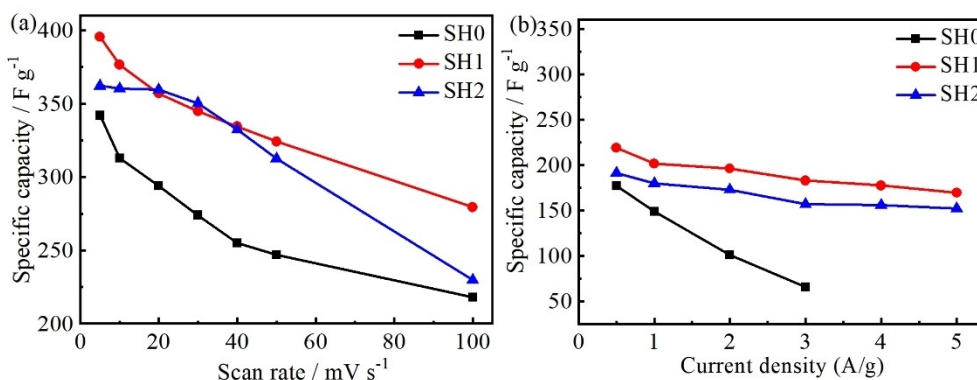

Figure 7. (a) Graph of scan rates and specific capacitances of SH0, SH1 and SH2; (b) Graph of current densities and specific capacitances of SH0, SH1 and SH2.
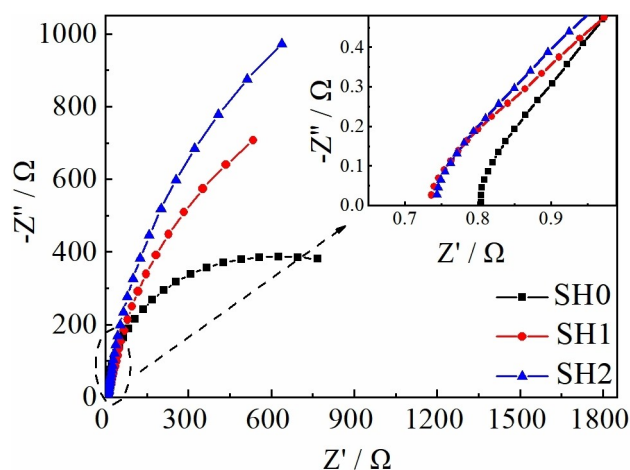
ChemistryOpen

Full Papers
doi.org/10.1002/open.202000206

Chemistry Europe
European Chemical
Societies Publishing

Figure 8. EIS of the compounds SH0, SH1 and SH2.

In the lower frequency region, due to the Warburg impedance, the curve presents a straight line approaching 90° in different degrees, which is related to the diffusion of ions in the electrolyte on the surface of the electrode material. By comparison, it can see that the curves of the SH1 and the SH2 are closer to the Y-axis, leading to a smaller resistance. Due to the existence of the equivalent series resistance (ESR), in the high-frequency region, the curve presents an insignificant semicircle. The resistance (R_s) value of 0.742 Ω for the SH1 or 0.752 Ω for the SH2 can be calculated from the intersection point between the curve and the real axis, which is less than that (0.803 Ω) of the SH0.

3. Conclusions

Upon introduction of axial substitution by m-hydroxybenzoic acid or m-hydroxyphenylacetic acid, two novel SubPcs (SH1 and SH2) were developed and well characterized. Besides the relatively higher fluorescence quantum efficiencies than that of the prototype Br-SubPc (SH0), the significantly enhanced specific capacitances and the larger capacitance retentions are also obtained for the SH1 and SH2. These results not only offer a synthetic route for the preparation of SubPc derivatives, but also show the potential of axial-substituted SubPcs for use as organic photovoltaics and supercapacitors.

Acknowledgements

Conflict of Interest

The authors declare no conflict of interest.

[1] J. L. Liu, C. B. Ouyang, F. Y. Huo, W. Q. He, A. C. Cao, *Dyes Pigm.* **2020**, *181*, 108509.
[2] H. Gommans, T. Aernouts, B. Verreet, P. Heremans, A. Medina, C. G. Claessens, T. Torres, *Adv. Funct. Mater.* **2009**, 19, 3435–3439.
[3] N. V. Shvedene, K. N. Otkidach, E. E. Ondar, M. M. Osipova, T. V. Dubinina, L. G. Tomilova, I. V. Pletnev, *J. Anal. Chem.* **2017**, *72*, 95–104.
[4] T. Huang, H. Chen, J. J. Feng, A. D. Zhang, W. Jiang, F. He, Z. H. Wang, *ACS Materials Lett.* **2019**, *1*, 404–409.
[5] X. S. Huang, M. Hu, X. H. Zhao, C. Li, Z. Y. Yuan, X. Liu, C. S. Cai, Y. D. Zhang, Y. Hu, Y. W. Chen, *Org. Lett.* **2019**, *21*, 3382–3386.
[6] H. Gotfredsen, T. Holmstrom, A. V. Munoz, F. E. Storm, C. G. Tortzen, A. Kadziola, K. V. Mikkelsen, O. Hammerich, M. B. Nielsen, *Org. Lett.* **2018**, *20*, 5821–5825.
[7] G. Bressan, A. N. Cammidge, G. A. Jones, I. A. Heisler, D. G. Lucas, S. R. Buenamanana, S. R. Meech, *J. Phys. Chem. A* **2019**, *123*, 5724–5733.
[8] P. J. Swarts, J. Conradie, *Electrochimica Acta* **2020**, *329*, 135165.
[9] Y. X. Li, H. K. M. Sheriff, X. Liu, C. Wang, K. Ding, H. Han, K. Wong, S. R. Forrest, *J. Am. Chem. Soc.* **2019**, *141*, 18204–18210.
[10] D. S. Josey, G. L. Ingram, R. K. Garner, J. M. Wang, G. J. Evans, Z. Lu, T. P. Bender, *ACS Appl. Energy Mater.* **2019**, *2*, 979–986.
[11] K. L. Sampson, X. Q. Jiang, E. Bukuroshi, A. Dovijarski, H. Raboui, T. P. Bender, K. M. Kadish, *J. Phys. Chem. A* **2018**, *122*, 4414–4424.
[12] E. R. L. Brisson, S. P. Andrew, E. M. Graham, T. P. Bender, *Ind. Eng. Chem. Res.* **2011**, *50*, 10910–10917.
[13] E. Caballero, J. Fernandez-Ariza, V. M. Lynch, C. Romero-Nieto, M. S. Rodriguez-Morgade, J. L. Sessler, D. M. Guldi, T. Torres, *Angew. Chem. Int. Ed.* **2012**, *51*, 11337–11342.
[14] Y. M. Wang, S. Mori, H. Furuta, S. Shimizu, *Angew. Chem.* **2019**, *131*, 11091–11095.
[15] C. Lakshmi, K. Viswanath, L. D. Shirtcliff, K. D. Berlin, *J. Porphyr. Phthalocya.* **2013**, *17*, 1167–1172.
[16] A. V. Munoz, H. Gotfredsen, M. Jevric, A. Kadziola, O. Hammerich, M. B. Nielsen, *J. Org. Chem.* **2018**, *83*, 2227–2234.
[17] J. S. Lissau, A. V. Munoz, H. Gotfredsen, M. Jevric, M. B. Nielsen, T. I. Solling, *J. Phys. Chem. A* **2018**, *122*, 6683-6692.
[18] E. Maligaspe, M. R. Hauwiller, Y. V. Zatsikha, J. A. Hinke, P. V. Solntsev, D. A. Blank, V. N. Nemykin, *Inorg. Chem.* **2014**, *53*, 9336–9347.
[19] C. G. Claessens, D. González-Rodríguez, T. Torres, *Chem. Rev.* **2002**, *102*, 835–853.
[20] S. Ardizzone, G. Fregonara, S. Trasatti, *Electrochim. Acta* **1990**, *35*, 263–267.
[21] D. G. Rodrıguez, T. Torres, D. Guldi, J. Rivera, M. A. Herranz, L. Echegoyen, *J. Am. Chem. Soc.* **2004**, *126*, 6301–6313.
[22] J. Yan, S. H. Li, B. B. Lan, Y. C. Wu, P. S. Lee, *Adv. Funct. Mater.* **2020**, *30*, 1902564.